

1        **NH<sub>3</sub> sensing with self-assembled ZnO-**  
2        **nanowire  $\mu$ HP sensors in isothermal and**  
3        **temperature-pulsed mode**

4  
5        F. Shao <sup>a, b, \*</sup>, J. D. Fan <sup>a, c</sup>, F. Hernández-Ramírez <sup>a, d, \*</sup>, C. Fàbrega <sup>a</sup>, T. Andreu <sup>a</sup>, A. Cabot <sup>a</sup>, J.  
6        D. Prades <sup>d</sup>, N. López <sup>e</sup>, F. Udrea <sup>f, g</sup>, A. De Luca <sup>f</sup>, S. Z. Ali <sup>g</sup>, J. R. Morante <sup>a, d</sup>

7  
8        <sup>a</sup> Catalonia Institute for Energy Research (IREC), Sant Adrià del Besòs E-08930, Spain

9        <sup>b</sup> School of Electronic Science and Engineering, Nanjing University, Nanjing 210023, China

10        <sup>c</sup> Clarendon Laboratory, University of Oxford, Parks Road, Oxford OX1 3PU, United Kingdom

11        <sup>d</sup> Department of Electronic, University of Barcelona, Barcelona E-08028, Spain

12        <sup>e</sup> Institute of Chemical Research of Catalonia (ICIQ), Tarragona 43007, Spain

13        <sup>f</sup> Department of Engineering, University of Cambridge, Cambridge, United Kingdom

14        <sup>g</sup> Cambridge CMOS Sensors Ltd, Cambridge, United Kingdom

15

16

17

18

19        \* Author to whom correspondence should be addressed: [fengangelo@hotmail.com](mailto:fengangelo@hotmail.com);

20        [fhernandez@irec.cat](mailto:fhernandez@irec.cat)

21        Tel: +86 13862251871

22 **Abstract**

23 Dielectrophoretic alignment is found to be a simple and efficient method to deposit the solution  
24 prepared ZnO nanowires onto micro hot plate substrates. Due to the strong surface effects,  
25 positive temperature coefficient for resistance was encountered with ZnO nanowires in the high  
26 temperature range ( $>250^{\circ}\text{C}$ ). The response to ammonia ( $\text{NH}_3$ ) was evaluated in isothermal and  
27 temperature-pulsed operation mode; the relative higher response observed in the latter case  
28 demonstrates that the use of this methodology is a good strategy to improve the performance of  
29 metal oxide sensors based on nanomaterials. Here, we evaluate the response to  $\text{NH}_3$  and  
30 qualitatively describe the sensing mechanism in temperature-pulsed mode, highlighting the main  
31 differences compared to the standard isothermal methodology.

32

33

34

35 **Key words:** ZnO; nanowire; micro hot plate; ammonia; gas sensor; temperature-pulsed

36

37

38

39

40

41

42

## 43 **1. Introduction**

44 Silicon on insulator (SOI) [1] technology offers the possibility of fabricating mono-crystalline  
45 silicon electronics with good thermal isolation. Micro hot plates ( $\mu$ HPs) based on standard  
46 complementary metal oxide semiconductor (CMOS) processing technology [2] using tungsten  
47 (W) metallization [3] and/or the SOI layer for the micro-heater are an ideal choice of substrates  
48 for resistive metal oxides (MOX) gas sensors. In addition to the very low power consumption  
49 (tens of mW in DC operation) and fast thermal response (tens of ms) [3], they can be cost  
50 effectively manufactured in high volume and integrated with other functional electronics [4, 5].  
51 On top of the  $\mu$ HPs (above the micro-heater), inter digital electrodes (IDEs) are usually patterned  
52 to monitor the resistance variation in the sensing layer during the change of gas compositions at  
53 the elevated temperature. The size of the whole device is often mm  $\times$  mm and the dimensions of  
54 the IDEs above the heater are of hundreds of micrometers. The miniaturization of the devices  
55 creates however a challenge, i.e., the deposition of sensing materials onto the micro-heater  
56 membrane in an effective way [6].

57 Conventional non-localized deposition techniques, e.g., sputtering [7-9], evaporation [10], spray  
58 coating [11] or electro-spinning [12] have to be combined with lithography of a deposition  
59 window or alignment of shadow masks; whereas localized deposition techniques that utilize the  
60 internal micro-heater to activate the growth have to use vapor phase precursors [6]. And if seed  
61 layers are required for the localized growth, the non-localized techniques are again needed to  
62 first produce them [13-15]. In the case of high precision screen printing [16], the deposition has  
63 to be made before the backside etching of the membrane to avoid its damage, making it  
64 inconvenient to the user of post CMOS wafer stage. Another set of techniques are those based on  
65 the direct deposition of sensing materials presented in liquid form by micro droplet coating [17,

66 18] or ink-jet printing [19, 20]. Apart from preparing the stable material suspension and the  
67 dedicated apparatuses, these two techniques also lack the capability of manipulating  
68 nanomaterials, e.g., the alignment of nanowires.

69 Dielectrophoretic (DEP) technique has been used to manipulate nanomaterials [21-24],  
70 especially metal [25] and semiconductor [23, 26] nanowires. The DEP force arises from the  
71 polarization of non-charged elements in a non-uniform electric field and attracts the object to the  
72 electrodes. It has been successfully applied to align nanowires [25, 27] or nanorods [28, 29] onto  
73 different substrates for later sensing purposes, and it is suggested to be fully compatible with the  
74 standard CMOS technology for wafer-scale implementation [30, 31].

75 MOXs are the most typical compounds studied and used as low cost resistive sensing materials.  
76 ZnO nanowires in particular have been identified as potential candidates to fabricate new devices  
77 [32]. Although ZnO nanowire-based gas sensors have been intensively studied in the last few  
78 years and promising results have been demonstrated [33-35], improvements are still needed to  
79 bring them into the commercial stage. On the other hand,  $\mu$ HP gas sensors are often investigated  
80 under the so-called temperature-programmed/modulated operation mode [36-40]. In this  
81 approach, the sensors are subjected to pulses of different temperatures and duration, instead of  
82 keeping the sensors' temperature at constant. Improvement of the sensors' selectivity and even  
83 quantification of gases [41, 42] can be achieved by pattern reading and data analysis. A variant to  
84 that is the so called temperature-pulsed operation mode [18, 41, 43, 44], in which the  
85 temperature of the sensor is constantly changed between two values (low and high) every few  
86 seconds and the resistance variation due to analyte gas at the low or high temperature end define  
87 the sensor response. With this approach, the sensitivity enhancement at the low temperature end  
88 is usually found.

89 In this work, the material deposition onto  $\mu$ HPs was further developed by applying the DEP  
90 alignment of ZnO nanowires at the post CMOS wafer stage. The gas sensing performance of the  
91 devices were tested with  $\text{NH}_3$  in both conventional isothermal and temperature-pulsed sensing  
92 modes. The mechanism that lies behind the enhanced sensing performance in the temperature-  
93 pulsed mode is qualitatively discussed.

94

## 95 **2. Experimental**

### 96 *2.1 Nanowire preparation*

97 ZnO nanowires were obtained by a hydrothermal process reported earlier [45]. In brief, an 80 nm  
98 thick of ZnO seed layer were first sputtered onto indium doped tin oxide (ITO) glass. The ITO  
99 glass was then placed in the growth solution that consist of 0.02 M zincnitrate, 0.015 M  
100 hexamethylenetetramine (HMTA), 0.004 M polyethyleneimine (end-capped, molecular weight  
101 800g/mol) and 0.024 M ammonium hydroxide. The solution was heated to 88°C, and after 3 h,  
102 ZnO nanowires grew to about 6 $\mu$ m in length with diameters ranges between 50 to 300 nm. The  
103 resulting ZnO arrays were rinsed with Mili-Q water and dried with nitrogen flow. More  
104 characterization results with, e.g., x-ray diffraction (XRD), scanning electron microscopy (SEM)  
105 can be found in ref.[45]. The solution of ZnO nanowires was obtained by sonicating the ITO  
106 substrate in isopropanol.

### 107 *2.2 The $\mu$ HPs*

108  $\mu$ HPs were obtained from Cambridge CMOS Sensors ([www.ccmoss.com](http://www.ccmoss.com)) [5]. The  $\mu$ HPs used in  
109 this work have IDEs made of gold (Au). Au is inert to oxidation and the rough Au surface  
110 provides good attachment to the later deposited nanowires. As shown in Fig.1a, the IDEs span a

111 circular area of 250  $\mu\text{m}$  in diameter and the gap between the IDE fingers is 10  $\mu\text{m}$ . The heating  
112 element made of W is buried under the IDEs within the  $\text{SiO}_2$  insulation. W is used as an  
113 interconnect metal in high temperature CMOS processes and has better stability and lower  
114 mechanical stress compared to poly-Si heaters. The circular  $\text{SiO}_2$  insulating membrane obtained  
115 by deep reactive ion etching (DRIE) has a diameter of 640  $\mu\text{m}$  and a thickness of about 5  $\mu\text{m}$ .  
116 Several Au bond pads that connect to the heater or IDEs are manufactured on the two sides of the  
117 chips for wire bonding. The maximum temperature the  $\mu\text{HPs}$  can reach is about 700°C, while the  
118 power consumption is only about 55 mW at 450°C.

### 119 *2.3 DEP assembly of nanowires*

120 The  $\mu\text{HP}$  chips were glued onto the transistor outline packages (TO-8) and wire bonded with Au  
121 wires (Fig. S1). The devices were then attached to a printed circuit board for ZnO nanowire  
122 deposition and later tests. ZnO nanowire solution in isopropanol was briefly sonicated before use.  
123 A micropipette was used to apply 2 drops ( $\sim 2.5\mu\text{l}$  each) of it onto the  $\mu\text{HPs}$  when the AC  
124 potential was applied on the IDEs by a function generator (TG2000, TTI). The voltage applied  
125 was 15  $V_{\text{p-p}}$  in square wave at the frequency of 5 MHz. Once the solvent had evaporated, the AC  
126 signal was turned off. The morphology of aligned nanowires on  $\mu\text{HPs}$  was examined using a  
127 SEM (Auriga, Zeiss). As the annealing/sintering step, the temperature of the  $\mu\text{HPs}$  was raised to  
128 400°C in stepwise and dwelled for 2 h.

### 129 *2.4 Gas sensing tests*

130 Gas sensing tests were performed with a homemade stainless steel chamber. Gas mixtures were  
131 introduced with thermal mass flow controllers (Bronkhost) by mixing the synthetic air (SA) with  
132  $\text{NH}_3$  in SA from the certified gas cylinders (Carburros Metálicos). The total flow rate was always

133 maintained at 200 ml/min. The micro-heater was powered by a source meter (2400, Keithley).  
134 For temperature-pulsed measurement, the pulsed voltage was in square waves and has a period  
135 of 10 s, i.e., the temperature of sensor changed between the low and high regime every 5 s. The  
136 settle time of both rise and fall of the pulsed input voltage were measured to be within 50 ms.  
137 Electrical measurements were made with another source meter (2635A, Keithley).

138

### 139 **3. Results and discussion**

#### 140 *3.1 The assembled device*

141 From the microscope images (Fig. 1b&c), we see that most of the nanowires were attached to the  
142 IDEs after the DEP process. The rest of the membrane surface was clean, and the small amount  
143 of nanowires left on the membrane presumably does not affect the overall performance of the  
144 device. As it is shown in Fig. 1c and Fig. S2, both the finger tips and the outmost of the IDEs had  
145 attracted the nanowires more efficiently compared to the center area. This result might arise from  
146 the interference presented at the center area when multiple IDEs fingers with an opposite  
147 potential were located very close to each other. The potential interference from nearby IDEs  
148 fingers can offset the polarization and attraction effects on the nanowires, leaving the center with  
149 fewer nanowires. SEM image in Fig. 2 shows that nanowires were aligned into bundles and  
150 interconnected to each other. Since their lengths are shorter than the gap between the IDEs,  
151 multiple nanowires are required to bridge the gap. Comparing to the nanowires that grow  
152 vertically on the membrane [13-15] and only having their bottom parts in contact with the  
153 membrane, the direct lying of nanowires on the  $\mu$ HP membrane offers better heat transfer  
154 property between the membrane and nanowires. This assures the annealing/sintering step can be

155 used to strength the connections between the nanowires or nanowire-electrodes. The finally  
156 obtained structures were proved to be stable, since no direct evidence of degradation or change  
157 of their properties was found after regularly testing and handling. This suggests that the bond  
158 strength among nanowires and nanowire-electrodes are strong enough to fabricate functional  
159 devices following our approach.

### 160 *3.2 Electrical properties*

161 The contact between semiconductor and metal can be either ohmic or rectifying depending on  
162 whether a Schottky barrier is present. Ideally, ohmic contact is obtained with n-type  
163 semiconductor if the work function of the metal is close or smaller than the electron affinity of  
164 the semiconductor [46]. In our case, Au has a work function of  $5.1\pm 0.1\text{eV}$  [47] which is larger  
165 than the theoretical electron affinity of ZnO ( $\sim 4.2\text{eV}$ ) [46]. The room temperature (RT) I-V  
166 curves (inset in Fig. 3a) of the annealed/sintered devices were found non-linear, indicating thus  
167 the formation of Schottky barrier at the Au-ZnO interface. The Schottky barrier however could  
168 be overcome by increasing the temperature [48]. The I-V curves became linear at  $200^\circ\text{C}$  and  
169 above, so the contact resistance contribution can be neglected in the later gas sensing  
170 measurements at high temperature.

171 The current values in I-V tests were found to increase with temperature until  $300^\circ\text{C}$  and then  
172 slightly declined at higher temperatures (Fig. 3a). These two opposite trends correspond to the  
173 negative (NTC) and positive temperature coefficients (PTC) of resistance, respectively. The  
174 negative one at low T results from the thermal generation of charge carriers and the overcoming  
175 of the Schottky and nanowire-nanowire junction barriers by electrons. On the other hand, the  
176 PTC after  $300^\circ\text{C}$  resembles the results reported for ZnO thin films by Min et al. [9, 49] and



177 shows the same tendency as those reported for ZnO nanorods [50] and nanofibers [51] in a  
178 slightly varied temperature range. The resistance was further measured with increasing the  
179 temperature in steps (Fig. 3b). The resistance was found to decrease along with the temperature  
180 rise until 250°C and only small drifts were observed during the dwell period. When the  $\mu$ HP  
181 temperature were raised to higher values, immediate drop of resistance were followed by drastic  
182 increase in the dwell period. The final resistance at 300°C has surpassed 250°C and even higher  
183 resistances were reached above this threshold. Such gradual increase of resistance also indicates  
184 that the I-V measurements are dependent on both the temperature and the dwell time at that  
185 temperature. As the I-V results in Fig. 3a were obtained about 1-2 minutes after the temperature  
186 adjustment, it follows the order of  $R(250^\circ\text{C}) > R(400^\circ\text{C}) > R(350^\circ\text{C}) > R(300^\circ\text{C})$ , which is  
187 consistent with Fig. 3b only in the non-stabilized region right after the temperature change  
188 (marked with circles in Fig. 3b). Moreover, the more stabilized region in Fig. 3b with  $R(400^\circ\text{C}) >$   
189  $R(350^\circ\text{C}) > R(300^\circ\text{C}) > R(250^\circ\text{C})$  is consistent with Fig. 4 in the next section.

190 Regarding the origin of the PTC phenomenon, we first exclude the possibility of bulk chemical  
191 structure or composition change as the nanowires were pre-annealed and had experienced long  
192 hours of repeated gas sensing tests at high temperatures, in which we have seen a stabilized  
193 resistance base line. Furthermore, the nanowire-electrode contacts were shown to be ohmic at the  
194 elevated temperatures, making no contribution to the measured resistance. ZnO nanowires  
195 studied here also do not satisfy the two well-known PTC effects caused by interfaces: the PTC  
196 effect in ferroelectric ceramic materials [52] and the PTC effect in composite oxides materials  
197 [53]. On the other hand, due to the strong surface dependence of nanomaterials, the cause of the  
198 PTC in MOX nanomaterials has been ascribed to the complex dynamics of thermal desorption of  
199 water and related hydroxyl group (-OH) or generation of charged atomic O species ( $\text{O}^-/\text{O}^{2-}$ ) on

200 the surface [9, 49-51, 54, 55]. For oxygen, the adsorbed molecular  $O_2^-$  dissociate in to  $O^-$  and  $O^{2-}$   
201 at high temperatures, which apparently withdraw the electron more efficiently. And for the  
202 chemisorbed  $H_2O$  and its by-product  $-OH$ , they act as the electron donor to the oxides, lowering  
203 the resistance at low temperature and increasing the resistance when removed by high  
204 temperature. Considering the high defect density of the solution prepared ZnO nanowires, the  
205 defects may have strong influence on their properties and have deeply involved in the as  
206 mentioned surface chemistries. Nevertheless, as will be shown next, despite the presence of the  
207 PTC, it doesn't undermine the capability of ZnO nanowires for gas sensing.

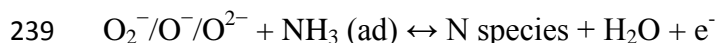
### 208 3.3 $NH_3$ sensing

209  $NH_3$  sensing tests were first performed at temperatures between  $200^\circ C$  and  $400^\circ C$  in the  
210 isothermal mode. As shown in Fig. 4, the response baseline in SA was fixed after the complete  
211 stabilization of the electrical resistance following a change in  $T$ . For this reason and in agreement  
212 with the abovementioned positive temperature coefficient of the devices, the initial resistance  
213 was found to slightly increase from  $300^\circ C$  and above. In all cases, nanowires responded to  $NH_3$   
214 by decreasing the resistance and the change was reversible when  $NH_3$  was purged from the  
215 chamber. The decrease of the resistance upon exposure to  $NH_3$  was expected as ZnO is an n-type  
216 semiconductor and  $NH_3$  is a reducing gas. Here we define the isothermal mode response  $S_{iso}$  to be  
217  $R_{SA}/R_{gas}$ , where  $R_{SA}$  and  $R_{gas}$  are the resistance values in SA and in gas mixture, respectively.  
218 Response and recovery time ( $t_{res}$  and  $t_{rev}$ ) were counted as the time it took to complete 90% of the  
219 total resistance change. The optimal working temperature for  $NH_3$  ( $S_{iso} = 4.2$  for 200 ppm; 2.3 for  
220 50 ppm and 1.5 for 10 ppm) was found to be  $350^\circ C$  (Fig. 5). At this temperature,  $t_{res}$  were 7.4,  
221 6.4 and 3.8 min for 10, 50 and 200 ppm of  $NH_3$ , and the corresponding  $t_{rev}$  were 18.4, 19.9 and

222 21.5 min, respectively. All these values are however convoluted with the dynamics of the  
223 chamber.

224 A survey of literature reported resistive nano-sensors is given in table S1 of the supplementary  
225 material. The  $S_{iso}$  value here obtained is found comparable to other studies of similar materials  
226 [56-58]. Indeed, the dependence of the gas response with the nanowires diameter is a well-  
227 known effect [35]; the response clearly benefits from the smaller diameters. This is more  
228 significant with thickness approaching to the Debye length. Herein, ZnO nanowires with  
229 diameters between 50 and 300 nm were tested and the thicker nanowires are believed to be the  
230 major current pathway. So the nanowires diameter is not favored by the high response and  
231 improvement can be simply made by making more uniform and thinner nanowires.

232 The  $\text{NH}_3$  response of ZnO nanowires can be explained using the classic model [59] of MOX gas  
233 sensors: the surface oxygen species (molecular  $\text{O}_2^-$  and atomic  $\text{O}^-$ ,  $\text{O}^{2-}$ ) withdraw electrons from  
234 the ZnO, creating a depletion region that acts as a non-conductive region at the surface and  
235 charge transfer barrier between the nanowire junctions (as shown in Fig. 6). When the  $\text{NH}_3$  is  
236 present, surface reaction occurs between the surface oxygen species and the adsorbed  $\text{NH}_3$   
237 molecule. These complex surface reactions can be simply described by the following equation  
238 [60]:



240 With  $\text{N}_2$  as the main reaction product, electrons are released by the surface reactions and the  
241 resistance of ZnO decreases. In more specific, ohmic contacts formation was previously  
242 confirmed between nanowires and electrodes at the elevated temperatures. So the measured  
243 resistance is composed of the resistance of nanowire themselves ( $R_{\text{nanowire}}$ ) and the resistance at

244 nanowire-nanowire junctions ( $R_{\text{junction}}$ ). As illustrated in Fig. 6, the surface reactions release the  
245 electrons back into the nanowires, causing the reduction of depletion region width and lowering  
246 of junction potential barriers. The two contributors of the total resistance,  $R_{\text{nanowire}}$  and  $R_{\text{junction}}$  are  
247 therefore both lowered and finally lead to the reduction of the measured resistance.

248 In Fig. 4, it can be noted that the resistance indeed showed upward shifting after a prior drop at  
249 the 10 ppm response of 400°C. And the recovered resistance after 10, 50 ppm exposure exceeded  
250 the base value. Such character could be ascribed to the generation of  $\text{NO}_2$  in addition to  $\text{N}_2$  by the  
251 surface reactions; as  $\text{NO}_2$  is considered to get adsorbed on the surface and withdraws electron  
252 [40, 61, 62]. The reason it appeared only at the low  $\text{NH}_3$  level and highest temperature might be  
253 the request on high energy and selectively producing of  $\text{NO}_2$  [57]. Moreover, the counter-  
254 balancing effect of  $\text{NH}_3$  might also cause it to be more visible at the low  $\text{NH}_3$ . All in all, the  
255 ammonia response follows a typical bell-shaped curve (Fig.5), which reveal that ammonia  
256 sensing is (i) a thermally activated process but also that (ii) the response (reaction rate) is given  
257 by the ammonia adsorption-reaction probabilities at the surface, following a non-linear  
258 dependence of the sensor output with increasing concentration. Actually, this behavior was  
259 explained by Ahlers et al. [63] in terms of competing phenomena described by two energetic  
260 parameters: the strength of Langmuir adsorption  $E_{\text{ads}}$  of  $\text{NH}_3$  molecules at the surface, and the  
261 activation energy for the combustion reaction  $E_{\text{RES}}$ . These two factors are thus the decisive  
262 parameters to explain the high-temperature drop-off of the sensitivity  $S$ . It must be pointed out  
263 that between 350°C and 400°C the response starts to decrease.

264 In the temperature-pulsed mode, the sensor temperature was continuously changed between a  
265 low (200°C or 250°C) and a higher value for every 5 s. The resistance of the nanowires was  
266 simultaneously recorded when the gas flow was switched from pure SA to 200 ppm  $\text{NH}_3$  in SA

267 and then purged back to SA. The resistance in the low temperature end was used to calculate the  
268 corresponding response  $S_{pulsed,low}$ . As shown in the Fig. 7, when the sensors were operated in the  
269 temperature-pulsed mode, the low or high end resistance no more equals to that in the isothermal  
270 mode of same temperature. And only the negative temperature coefficient was observed when  
271 changing the temperature in short pulses. A significant enhancement of response  $S_{pulsed,low}$   
272 compared to the isothermal mode of same temperature was observed. For 200°C or 250°C as the  
273 low end temperature, the response  $S_{pulsed,low}$  increased with the high end temperature following a  
274 linear dependence (Fig. 8a). And the response  $S_{pulsed,low}$  of a particular high end temperature were  
275 highly approximate to each other. This indicates that in this mode,  $S_{pulsed,low}$  is determined by the  
276 high end temperature. The relative response compared to that of the isothermal mode was  
277 calculated as  $\Delta S = (S_{pulsed,low} - S_{iso,low})/S_{iso,low} * 100\%$  and given in Fig. 8b. Here,  $S_{iso,low}$  is the  
278 isothermal response in the corresponding temperature. From the tests,  $\Delta S$  with 200°C as the low  
279 end temperature were found to be always higher than that of 250°C, indicating that  $\Delta S$  also  
280 increases with the difference between the high and the low end temperatures. Although strongly  
281 affected by the chamber volume and the gas flow rate, the response and recovery of the  
282 resistance also became faster in the pulsed mode (see Fig. S3). Overall, the low temperature end  
283  $t_{res}$  at the pulsed mode decreased with increasing high end temperature and the values are about  
284 on a par with that of the isothermal mode in the temperature same to the high end. An equivalent  
285 correlation was found for the recovery. Due to the fact that resistance did not recover completely  
286 within the given time (10 min), the recovery ratio ( $R_{end}/R_{SA} * 100\%$ , where  $R_{end}$  is the resistance  
287 when ending the SA refill) is defined. With pulsed temperature (especially at 300°C and 350°C  
288 high end  $T$ ), the recovery ratio of the pulsed mode increased to higher values.

289 Similar response enhancement effects in the temperature-pulsed mode operation of  $\mu$ HP gas  
290 sensors have been previously reported in several works [18, 41, 43, 44]. As the surface oxygen  
291 species play a key role in the sensing mechanisms of reducing gases, A. Heilig et al. [41],  
292 proposed that the enhancement is mainly caused by the presence of high temperature surface  
293 oxygen species, i.e.,  $O^-/O^{2-}$  [59] in the low temperature period, which would be less or not  
294 existed in the equivalent isothermal mode.  $O^-/O^{2-}$  are produced after the dissociation [64] of  
295 surface adsorbed molecular oxygen at high temperatures and remains there in the low  
296 temperature period due to the fast thermal transition of this mode. They strongly regulate the  
297 electron concentration near the surface and when surface reaction with reducing gas occurs,  
298 electrons will be released back to the surface to cause the resistance change. Furthermore, the  
299 higher reactivity of atomic  $O^-/O^{2-}$  with  $NH_3$  will also lead to the faster response and recovery  
300 processes.

301 As mentioned in ref. [18] and [39], the surface cleaning effect during the high temperature period  
302 could also be the reason behind the response enhancement. Here, for the  $NH_3$  sensing with ZnO  
303 nanowires, we propose two potential adsorbates that can deteriorate the performance of the  
304 sensor in isothermal mode and can be removed at high temperatures. The first is  $H_2O$  and its by  
305 product, hydroxyl group ( $-OH$ ).  $H_2O$  is a well-known substance that interferes the output of  
306 MOX gas sensors [65, 66].  $H_2O$  and its byproduct  $-OH$  has been appointed as one of the causes  
307 of positive temperature coefficient in the previous section. There are three sources of  $H_2O$  that  
308 can be adsorbed onto ZnO surface: i) when the sensor is exposed to ambient air at RT; ii) the  
309 trace level of  $H_2O$  presented in the SA; iii) the residual  $H_2O$  in the test chamber. The second  
310 adsorbate is  $NO_2$ , which was considered to be a secondary product of oxygen- $NH_3$  reaction at the  
311 surface and has a counter effect on  $NH_3$  sensing [40, 61, 62]. When operated in the temperature-

312 pulsed mode, the amount of H<sub>2</sub>O/-OH and NO<sub>2</sub> can be diminished during the high temperature  
313 period. Exposing the free surface active sites to O<sub>2</sub> and NH<sub>3</sub> at low temperature period will  
314 enable a higher response and faster surface sensing mechanisms. Fig. S4 shows, in a shorter time  
315 scale, the resistance of the device working in temperature-pulsed mode between 200 and 350°C  
316 in constant SA flow. As expected, the resistance was found to drift continuously in both high and  
317 low temperature period after a sudden large change due to the fast temperature switch. This  
318 indicates the material was in a meta-stable state, which is evidence to the as proposed sensing  
319 mechanism and the response enhancement.

320

#### 321 **4. Conclusions**

322 ZnO nanowires were successfully deposited onto CMOS SOI μHP substrates for gas sensing  
323 applications. By DEP, nanowires prepared from a wide range of methods can be readily  
324 integrated onto μHPs. When working in the pulsed mode, a significant enhancement in the NH<sub>3</sub>  
325 sensing performance was observed at the low temperature end. It is proposed that this  
326 phenomenon is not only related to the high temperature surface oxygen species but also to the  
327 modulation of H<sub>2</sub>O (-OH) and N<sub>2</sub>O on the surface. The combination of the highly advanced  
328 CMOS SOI μHPs with this operation mode provides a new option to obtain reliable low cost gas  
329 sensors with even lower power consumption and high response.

330

#### 331 **Acknowledgement**

332 The research was supported by the Framework 7 program under the project SOI-HIT (FP7-FP7-  
333 ICT-2011-7) and European Regional Development Funds (ERDF). Authors from IREC

334 acknowledge the financial support given by the XaRMAE Network of Excellence on Materials  
335 for Energy of the “Generalitat de Catalunya”. F.H.-R. also acknowledges the support of the  
336 DAAD (D/11/43761). J. Fan also thanks for the support of the Secretary for Universities and  
337 Research of the Ministry of Economy and Knowledge of the Government of Catalonia.

338



339 **References**

340 [1] T. Iwaki, J.A. Covington, J.W. Gardner, F. Udrea, C.S. Blackman, I.P. Parkin, SOI-CMOS based single  
341 crystal silicon micro-heaters for gas sensors, 2006 IEEE Sensors, (2007) 460-3.

342 [2] O. Brand, G.K. Fedder, CMOS-MEMS: Wiley-VCH; 2005.

343 [3] S.Z. Ali, F. Udrea, W.I. Milne, J.W. Gardner, Tungsten-Based SOI Microhotplates for Smart Gas  
344 Sensors, Journal of Microelectromechanical Systems, 17(2008) 1408-17.

345 [4] D. Barrettino, M. Graf, M. Zimmermann, C. Hagleitner, A. Hierlemann, H. Baltes, A Smart Single-Chip  
346 Micro-Hotplate-Based Gas Sensor System in CMOS-Technology, Analog Integrated Circuits and Signal  
347 Processing, 39(2004) 275-87.

348 [5] A. De Luca, V. Pathirana, S.Z. Ali, D. Dragomirescu, F. Udrea, Experimental, analytical and numerical  
349 investigation of non-linearity of SOI diode temperature sensors at extreme temperatures, Sensors and  
350 Actuators A: Physical, 222(2015) 31-8.

351 [6] S. Semancik, R.E. Cavicchi, M.C. Wheeler, J.E. Tiffany, G.E. Poirier, R.M. Walton, et al., Microhotplate  
352 platforms for chemical sensor research, Sensors and Actuators B: Chemical, 77(2001) 579-91.

353 [7] J. Wöllenstein, J.A. Plaza, C. Cané, Y. Min, H. Böttner, H.L. Tuller, A novel single chip thin film metal  
354 oxide array, Sensors and Actuators B: Chemical, 93(2003) 350-5.

355 [8] M. Stankova, X. Vilanova, J. Calderer, E. Llobet, J. Brezmes, I. Gràcia, et al., Sensitivity and selectivity  
356 improvement of rf sputtered WO<sub>3</sub> microhotplate gas sensors, Sensors and Actuators B: Chemical,  
357 113(2006) 241-8.

358 [9] Y. Min, H.L. Tuller, S. Palzer, J. Wöllenstein, H. Böttner, Gas response of reactively sputtered ZnO  
359 films on Si-based micro-array, Sensors and Actuators B: Chemical, 93(2003) 435-41.

360 [10] A. Friedberger, P. Kreisl, E. Rose, G. Müller, G. Kühner, J. Wöllenstein, et al., Micromechanical  
361 fabrication of robust low-power metal oxide gas sensors, Sensors and Actuators B: Chemical, 93(2003)  
362 345-9.

363 [11] I. Jiménez, A. Cirera, A. Cornet, J.R. Morante, I. Gracia, C. Cané, Pulverisation method for active  
364 layer coating on microsystems, Sensors and Actuators B: Chemical, 84(2002) 78-82.

365 [12] Y. Zhao, X. He, J. Li, X. Gao, J. Jia, Porous CuO/SnO<sub>2</sub> composite nanofibers fabricated by  
366 electrospinning and their H<sub>2</sub>S sensing properties, Sensors and Actuators B: Chemical, 165(2012) 82-7.

367 [13] S. Santra, S.Z. Ali, P.K. Guha, G.F. Zhong, J. Robertson, J.A. Covington, et al., Post-CMOS wafer level  
368 growth of carbon nanotubes for low-cost microsensors—a proof of concept, Nanotechnology, 21(2010)  
369 485301.

370 [14] S. Barth, R. Jimenez-Diaz, J. Sama, J. Daniel Prades, I. Gracia, J. Santander, et al., Localized growth  
371 and in situ integration of nanowires for device applications, Chemical Communications, 48(2012) 4734-  
372 6.

373 [15] S. Santra, P.K. Guha, S.Z. Ali, P. Hiralal, H.E. Unalan, J.A. Covington, et al., ZnO nanowires grown on  
374 SOI CMOS substrate for ethanol sensing, Sensors and Actuators B: Chemical, 146(2010) 559-65.

375 [16] E. Llobet, P. Ivanov, X. Vilanova, J. Brezmes, J. Hubalek, K. Malysz, et al., Screen-printed nanoparticle  
376 tin oxide films for high-yield sensor microsystems, Sensors and Actuators B: Chemical, 96(2003) 94-104.

377 [17] J. Puigcorbé, A. Cirera, J. Cerdà, J. Folch, A. Cornet, J.R. Morante, Microdeposition of microwave  
378 obtained nanoscaled SnO<sub>2</sub> powders for gas sensing microsystems, Sensors and Actuators B: Chemical,  
379 84(2002) 60-5.

380 [18] A.M. Ruiz, X. Illa, R. Díaz, A. Romano-Rodríguez, J.R. Morante, Analyses of the ammonia response of  
381 integrated gas sensors working in pulsed mode, Sensors and Actuators B: Chemical, 118(2006) 318-22.

382 [19] M.A. Andio, P.N. Browning, P.A. Morris, S.A. Akbar, Comparison of gas sensor performance of SnO<sub>2</sub>  
383 nano-structures on microhotplate platforms, Sensors and Actuators B: Chemical, 165(2012) 13-8.

384 [20] J. Kukkola, M. Mohl, A.-R. Leino, G. Toth, M.-C. Wu, A. Shchukarev, et al., Inkjet-printed gas sensors:  
385 metal decorated WO<sub>3</sub> nanoparticles and their gas sensing properties, *Journal of Materials Chemistry*,  
386 22(2012) 17878-86.

387 [21] H.Y. Yu, B.H. Kang, U.H. Pi, C.W. Park, S.-Y. Choi, G.T. Kim, V<sub>2</sub>O<sub>5</sub> nanowire-based nanoelectronic  
388 devices for helium detection, *Applied Physics Letters*, 86(2005) 253102-3.

389 [22] A.W. Maijenburg, M.G. Maas, E.J.B. Rodijk, W. Ahmed, E.S. Kooij, E.T. Carlen, et al.,  
390 Dielectrophoretic alignment of metal and metal oxide nanowires and nanotubes: A universal set of  
391 parameters for bridging prepatterned microelectrodes, *Journal of Colloid and Interface Science*,  
392 355(2011) 486-93.

393 [23] C.S. Lao, J. Liu, P. Gao, L. Zhang, D. Davidovic, R. Tummala, et al., ZnO Nanobelt/Nanowire Schottky  
394 Diodes Formed by Dielectrophoresis Alignment across Au Electrodes, *Nano Letters*, 6(2006) 263-6.

395 [24] E.M. Freer, O. Grachev, X. Duan, S. Martin, D.P. Stumbo, High-yield self-limiting single-nanowire  
396 assembly with dielectrophoresis, *Nat Nano*, 5(2010) 525-30.

397 [25] X. Li, Y. Wang, Y. Lei, Z. Gu, Highly sensitive H<sub>2</sub>S sensor based on template-synthesized CuO  
398 nanowires, *RSC Advances*, 2(2012) 2302-7.

399 [26] C. Leiterer, G. Broenstrup, N. Jahr, M. Urban, C. Arnold, S. Christiansen, et al., Applying contact to  
400 individual silicon nanowires using a dielectrophoresis (DEP)-based technique, *J Nanopart Res*, 15(2013)  
401 1-7.

402 [27] X. Li, Z. Gu, J. Cho, H. Sun, P. Kurup, Tin-copper mixed metal oxide nanowires: Synthesis and sensor  
403 response to chemical vapors, *Sensors and Actuators B: Chemical*, 158(2011) 199-207.

404 [28] W.J. Liu, J. Zhang, L.J. Wan, K.W. Jiang, B.R. Tao, H.L. Li, et al., Dielectrophoretic manipulation of  
405 nano-materials and its application to micro/nano-sensors, *Sensors and Actuators B: Chemical*, 133(2008)  
406 664-70.

407 [29] S.R. Mahmoodi, B. Raissi, E. Marzbanrad, N. Shojayi, A. Aghaei, C. Zamani, Dielectrophoretic  
408 assembly of ZnO nanorods for gas sensing, *Procedia Chemistry*, 1(2009) 947-50.

409 [30] A.H. Monica, S.J. Papadakis, R. Osiander, M. Paranjape, Wafer-level assembly of carbon nanotube  
410 networks using dielectrophoresis, *Nanotechnology*, 19(2008) 085303.

411 [31] S. Evoy, N. DiLello, V. Deshpande, A. Narayanan, H. Liu, M. Riegelman, et al., Dielectrophoretic  
412 assembly and integration of nanowire devices with functional CMOS operating circuitry, *Microelectronic  
413 Engineering*, 75(2004) 31-42.

414 [32] U. Ozgur, D. Hofstetter, H. Morkoc, ZnO Devices and Applications: A Review of Current Status and  
415 Future Prospects, *Proceedings of the IEEE*, 98(2010) 1255-68.

416 [33] Z. Fan, J.G. Lu, Gate-refreshable nanowire chemical sensors, *Applied Physics Letters*, 86(2005) -.

417 [34] M.W. Ahn, K.S. Park, J.H. Heo, D.W. Kim, K.J. Choi, J.G. Park, On-chip fabrication of ZnO-nanowire  
418 gas sensor with high gas sensitivity, *Sensors and Actuators B: Chemical*, 138(2009) 168-73.

419 [35] O. Lupan, V.V. Ursaki, G. Chai, L. Chow, G.A. Emelchenko, I.M. Tiginyanu, et al., Selective hydrogen  
420 gas nanosensor using individual ZnO nanowire with fast response at room temperature, *Sensors and  
421 Actuators B: Chemical*, 144(2010) 56-66.

422 [36] R.E. Cavicchi, J.S. Suehle, K.G. Kreider, M. Gaitan, P. Chaparala, Fast temperature programmed  
423 sensing for micro-hotplate gas sensors, *Electron Device Letters, IEEE*, 16(1995) 286-8.

424 [37] K.D. Benkstein, B. Raman, D.L. Lahr, J.E. Bonevich, S. Semancik, Inducing analytical orthogonality in  
425 tungsten oxide-based microsensors using materials structure and dynamic temperature control, *Sensors  
426 and Actuators B: Chemical*, 137(2009) 48-55.

427 [38] D.C. Meier, J.K. Evju, Z. Boger, B. Raman, K.D. Benkstein, C.J. Martinez, et al., The potential for and  
428 challenges of detecting chemical hazards with temperature-programmed microsensors, *Sensors and  
429 Actuators B: Chemical*, 121(2007) 282-94.

430 [39] A.P. Lee, B.J. Reedy, Temperature modulation in semiconductor gas sensing, *Sensors and Actuators  
431 B: Chemical*, 60(1999) 35-42.

432 [40] C. Bur, P. Reimann, A. Schutze, M. Andersson, A.L. Spetz, Increasing the selectivity of Pt-gate SiC  
433 field effect gas sensors by dynamic temperature modulation, *Sensors*, 2010 IEEE2010, pp. 1267-72.

434 [41] A. Heilig, N. Bârsan, U. Weimar, M. Schweizer-Berberich, J.W. Gardner, W. Göpel, Gas identification  
435 by modulating temperatures of SnO<sub>2</sub>-based thick film sensors, *Sensors and Actuators B: Chemical*,  
436 43(1997) 45-51.

437 [42] R. Gosangi, R. Gutierrez-Osuna, Active temperature modulation of metal-oxide sensors for  
438 quantitative analysis of gas mixtures, *Sensors and Actuators B: Chemical*, 185(2013) 201-10.

439 [43] M. Jaegle, J. Wöllenstein, T. Meisinger, H. Böttner, G. Müller, T. Becker, et al., Micromachined thin  
440 film SnO<sub>2</sub> gas sensors in temperature-pulsed operation mode, *Sensors and Actuators B: Chemical*,  
441 57(1999) 130-4.

442 [44] M. Schweizer-Berberich, S. Strathmann, U. Weimar, R. Sharma, A. Seube, A. Peyre-Lavigne, et al.,  
443 Strategies to avoid VOC cross-sensitivity of SnO<sub>2</sub>-based CO sensors, *Sensors and Actuators B: Chemical*,  
444 58(1999) 318-24.

445 [45] J. Fan, Y. Hao, A. Cabot, E.M.J. Johansson, G. Boschloo, A. Hagfeldt, Cobalt(II/III) Redox Electrolyte in  
446 ZnO Nanowire-Based Dye-Sensitized Solar Cells, *ACS Applied Materials & Interfaces*, 5(2013) 1902-6.

447 [46] L.J. Brillson, Y. Lu, ZnO Schottky barriers and Ohmic contacts, *Journal of Applied Physics*, 109(2011)  
448 121301-33.

449 [47] D.E. Eastman, Photoelectric Work Functions of Transition, Rare-Earth, and Noble Metals, *Physical*  
450 *Review B*, 2(1970) 1-2.

451 [48] F. Hernandez-Ramirez, A. Tarancon, O. Casals, E. Pellicer, J. Rodriguez, A. Romano-Rodriguez, et al.,  
452 Electrical properties of individual tin oxide nanowires contacted to platinum electrodes, *PhysRevB*,  
453 76(2007) 085429.

454 [49] Y. Ming, Properties and sensor performance of zinc oxide thin films: Massachusetts Institute of  
455 Technology; 2003.

456 [50] H. Guan-nan, H. Bo, S. Hui, Positive temperature coefficient of resistance of single ZnO nanorods,  
457 *Nanotechnology*, 22(2011) 065304.

458 [51] S. Wei, S. Wang, Y. Zhang, M. Zhou, Different morphologies of ZnO and their ethanol sensing  
459 property, *Sensors and Actuators B: Chemical*, 192(2014) 480-7.

460 [52] X.-w. Zhu, S.-w. Wang, S.-w. Zhong, Y.-y. Liu, S.-y. Shen, W.-z. Jiang, et al., PTCR effects in Sr-doped  
461 KNbO<sub>3</sub> ferroelectric ceramic materials, *Ceramics International*, 40(2014) 12383-6.

462 [53] D. Lisjak, M. Drofenik, D. Kolar, Composite ceramics with a positive temperature coefficient of  
463 electrical resistivity effect, *Journal of Materials Research*, 15(2000) 417-28.

464 [54] G. Neri, A. Bonavita, G. Micali, G. Rizzo, N. Pinna, M. Niederberger, In<sub>2</sub>O<sub>3</sub> and Pt-In<sub>2</sub>O<sub>3</sub>  
465 nanopowders for low temperature oxygen sensors, *Sensors and Actuators B: Chemical*, 127(2007) 455-  
466 62.

467 [55] X. Li, E. Chin, H. Sun, P. Kurup, Z. Gu, Fabrication and integration of metal oxide nanowire sensors  
468 using dielectrophoretic assembly and improved post-assembly processing, *Sensors and Actuators B:*  
469 *Chemical*, 148(2010) 404-12.

470 [56] S.J. Chang, W.Y. Weng, C.L. Hsu, T.J. Hsueh, High sensitivity of a ZnO nanowire-based ammonia gas  
471 sensor with Pt nano-particles, *Nano Communication Networks*, 1(2010) 283-8.

472 [57] Q. Qi, T. Zhang, L. Liu, X. Zheng, G. Lu, Improved NH<sub>3</sub>, C<sub>2</sub>H<sub>5</sub>OH, and CH<sub>3</sub>COCH<sub>3</sub> sensing properties  
473 of SnO<sub>2</sub> nanofibers by adding block copolymer P123, *Sensors and Actuators B: Chemical*, 141(2009) 174-  
474 8.

475 [58] C. Li, D. Zhang, B. Lei, S. Han, X. Liu, C. Zhou, Surface Treatment and Doping Dependence of In<sub>2</sub>O<sub>3</sub>  
476 Nanowires as Ammonia Sensors, *The Journal of Physical Chemistry B*, 107(2003) 12451-5.

477 [59] N. Barsan, U. Weimar, Conduction Model of Metal Oxide Gas Sensors, *J Electroceram*, 7(2001) 143-  
478 67.

479 [60] F. Shao, M.W.G. Hoffmann, J.D. Prades, J.R. Morante, N. López, F. Hernández-Ramírez, Interaction  
480 Mechanisms of Ammonia and Tin Oxide: A Combined Analysis Using Single Nanowire Devices and DFT  
481 Calculations, *The Journal of Physical Chemistry C*, 117(2013) 3520-6.  
482 [61] I. Jimenez, M.A. Centeno, R. Scotti, F. Morazzoni, A. cornet, NH<sub>3</sub> Interaction with Catalytically  
483 Modified Nano WO<sub>3</sub> Poders for Gas Sensing Applications, *J Electro Chem Soc*, 150(2003) 72-80.  
484 [62] Y. Shimizu, T. Okamoto, Y. Takao, M. Egashira, Desorption Behavior of Ammonia from TiO<sub>2</sub> based  
485 Specimens -Ammonia Sensing Mechanism of Double Layer Sensors with TiO<sub>2</sub> based Catalyst Layers, *J*  
486 *Mol Catal A: Chem*, 155(2000) 183-91.  
487 [63] S. Ahlers, G. Müller, T. Doll, A rate equation approach to the gas sensitivity of thin film metal oxide  
488 materials, *Sensors and Actuators B: Chemical*, 107(2005) 587-99.  
489 [64] J. Oviedo, M.J. Gillan, First-principles study of the interaction of oxygen with the SnO<sub>2</sub> (110) surface,  
490 *Surf Sci*, (2001) 221-36.  
491 [65] F.H. Ramirez, S. Barth, A. Tاراcon, O. Casals, E. Pellicer, J. Rodriguez, et al., Water Vapor Detection  
492 with Individual Tin Oxide Nanowires, *Nanotechnology*, 18(2007) 424016.  
493 [66] C.S. Rout, M. Hegde, A. Govindaraj, C.N.R. Rao, Ammonia sensors based on metal oxide  
494 nanostructures, *Nanotechnology*, 18(2007) 205504.

495

496

497

498

499

500

501

502

503

504

505

506

507

508

509 **Figure captions**

510 **Fig. 1.** (a) Layout of the CMOS SOI  $\mu$ HP substrate with gold IDEs. (b) The  $\mu$ HP substrate after wire  
511 bonding and nanowire deposition (ZnO nanowires appear in white under optical microscope). (c) Digital  
512 microscope image of the membrane after nanowire deposition (nanowires and IDEs both appear in deep  
513 colour).

514 **Fig. 2.** SEM image showing nanowires assembled between the IDEs (The right half is the magnified  
515 image of the area in the small box on the left side).

516 **Fig. 3.** (a) I-V curves of the annealed device at different temperatures, (inset) room temperature (RT) I-V  
517 curve. Note the measurements were made about 1-2 minutes after the temperature adjustment, the  
518 resistance order of  $R(250^\circ\text{C}) > R(400^\circ\text{C}) > R(350^\circ\text{C}) > R(300^\circ\text{C})$  can be retrieved. (b) Resistance variation  
519 with temperature increasing in steps (measured with probing current of 100 nA);  $\circ$ : non-stabilized region,  
520  $\square$ : stabilized region.

521 **Fig. 4.**  $\text{NH}_3$  sensing of the ZnO nanowire device in isothermal mode.

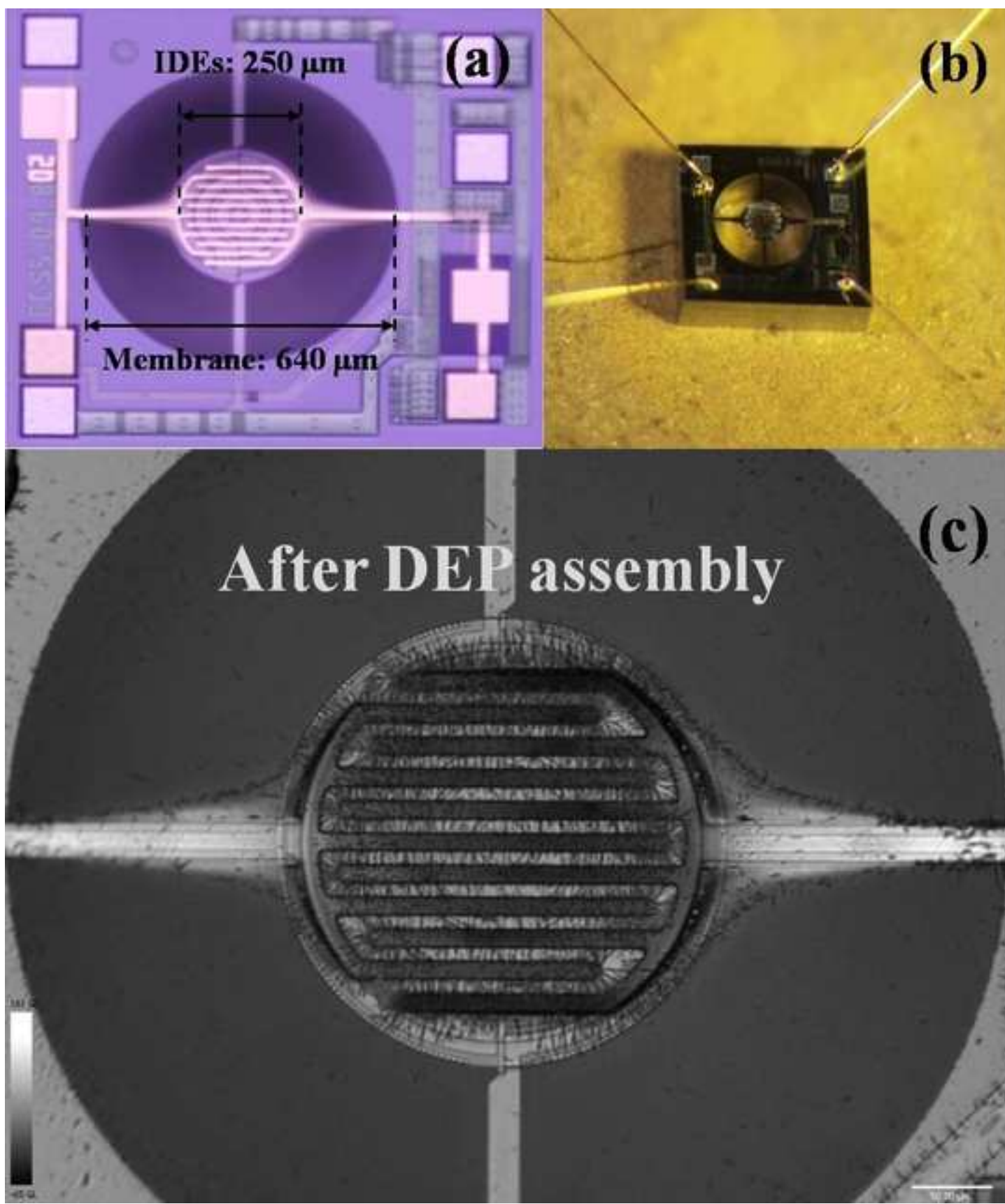
522 **Fig. 5.** Response vs.  $T$  of ZnO nanowires to different concentration of  $\text{NH}_3$  in isothermal mode ( $S_{iso} =$   
523  $R_{SA}/R_{gas}$ ).

524 **Fig. 6.** Schematic illustrating the mechanism of  $\text{NH}_3$  sensing.

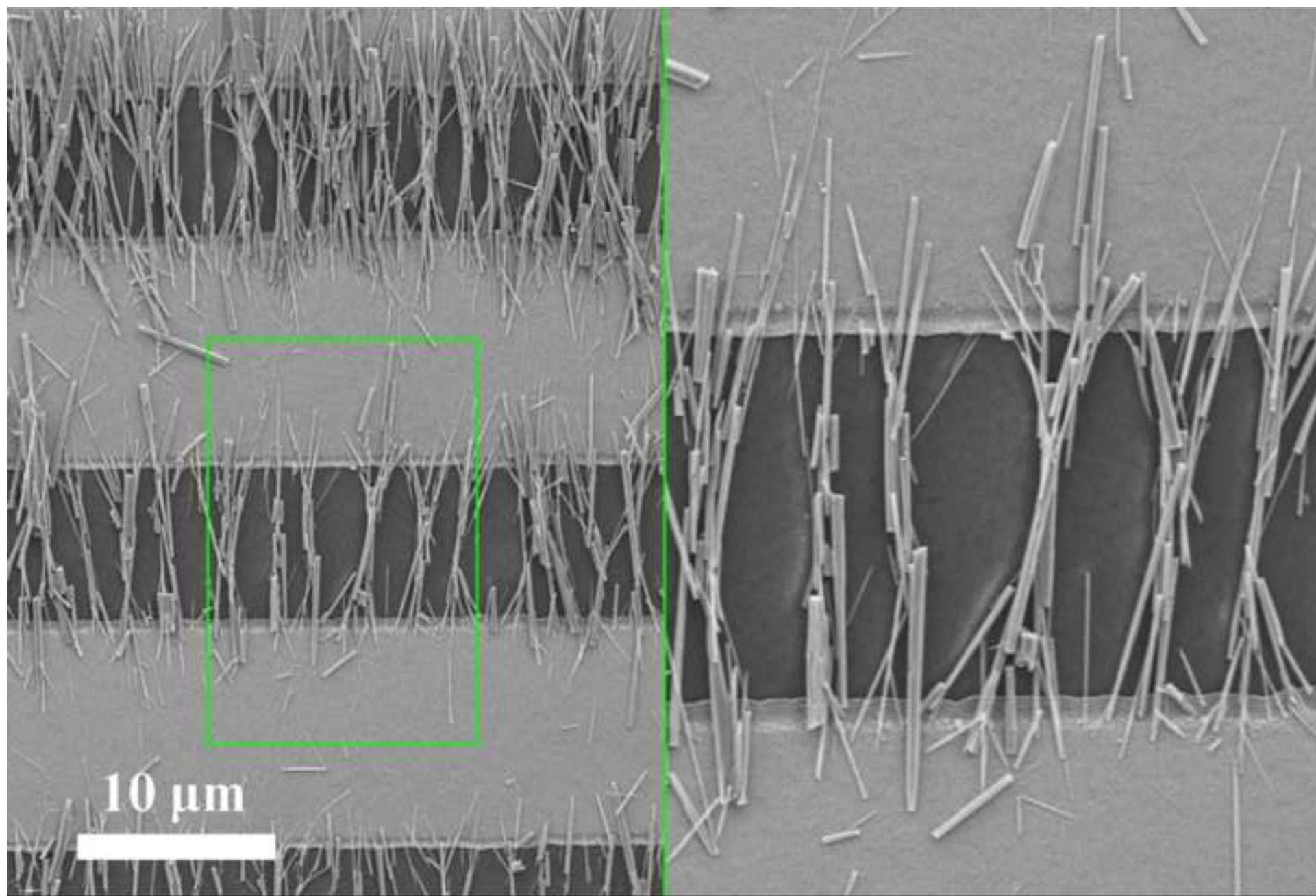
525 **Fig. 7.** Temperature-pulsed and isothermal sensing of 200 ppm  $\text{NH}_3$ .

526 **Fig. 8.** (a) Response  $S_{pulsed,low}$  for low end temperature of 200 and 250°C. (b) Relative response increase  
527  $\Delta S$ . The error bars represent the sample standard deviation of 3 measurements.

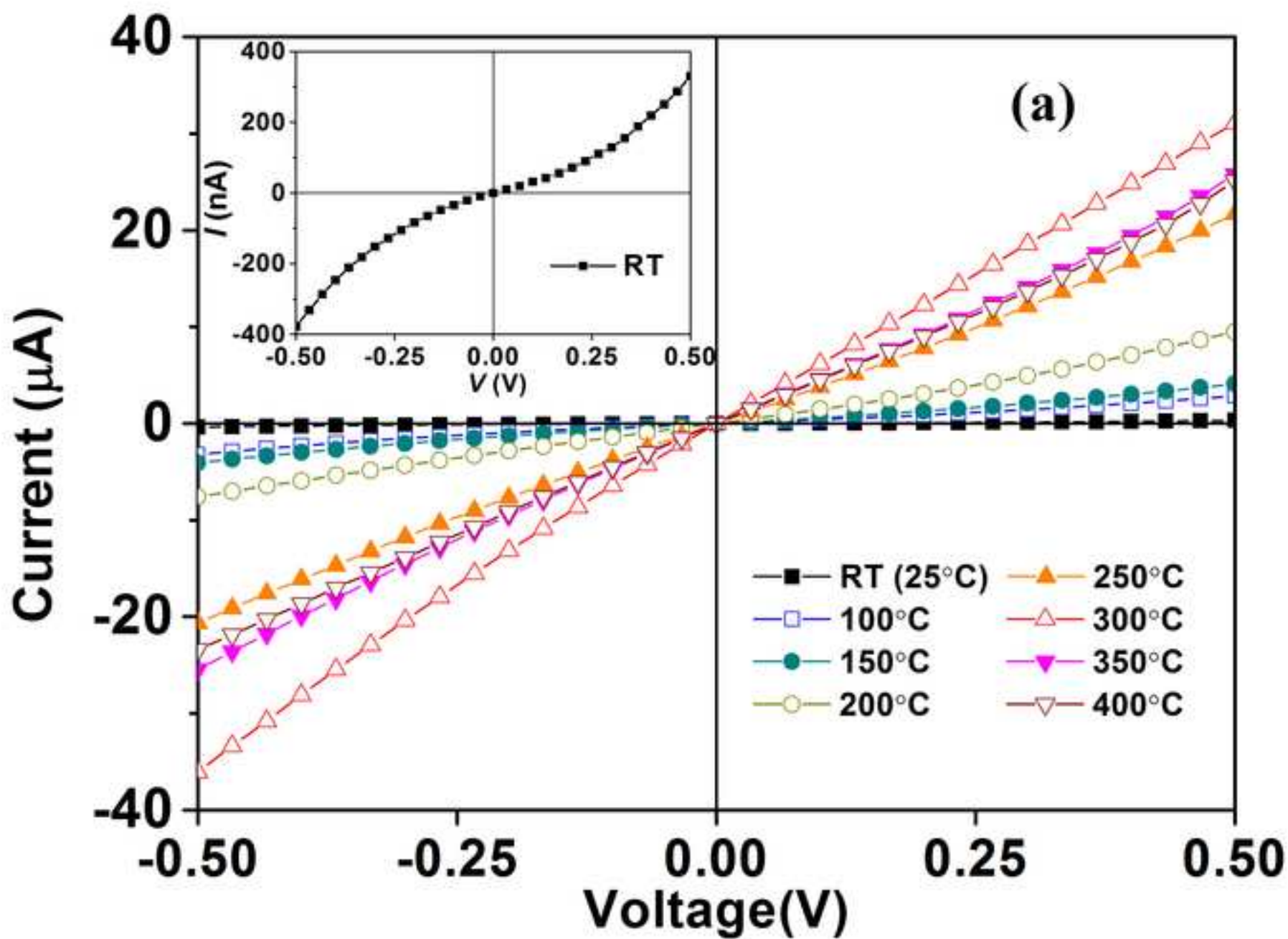
Figure(1)  
[Click here to download high resolution image](#)



Figure(2)  
[Click here to download high resolution image](#)

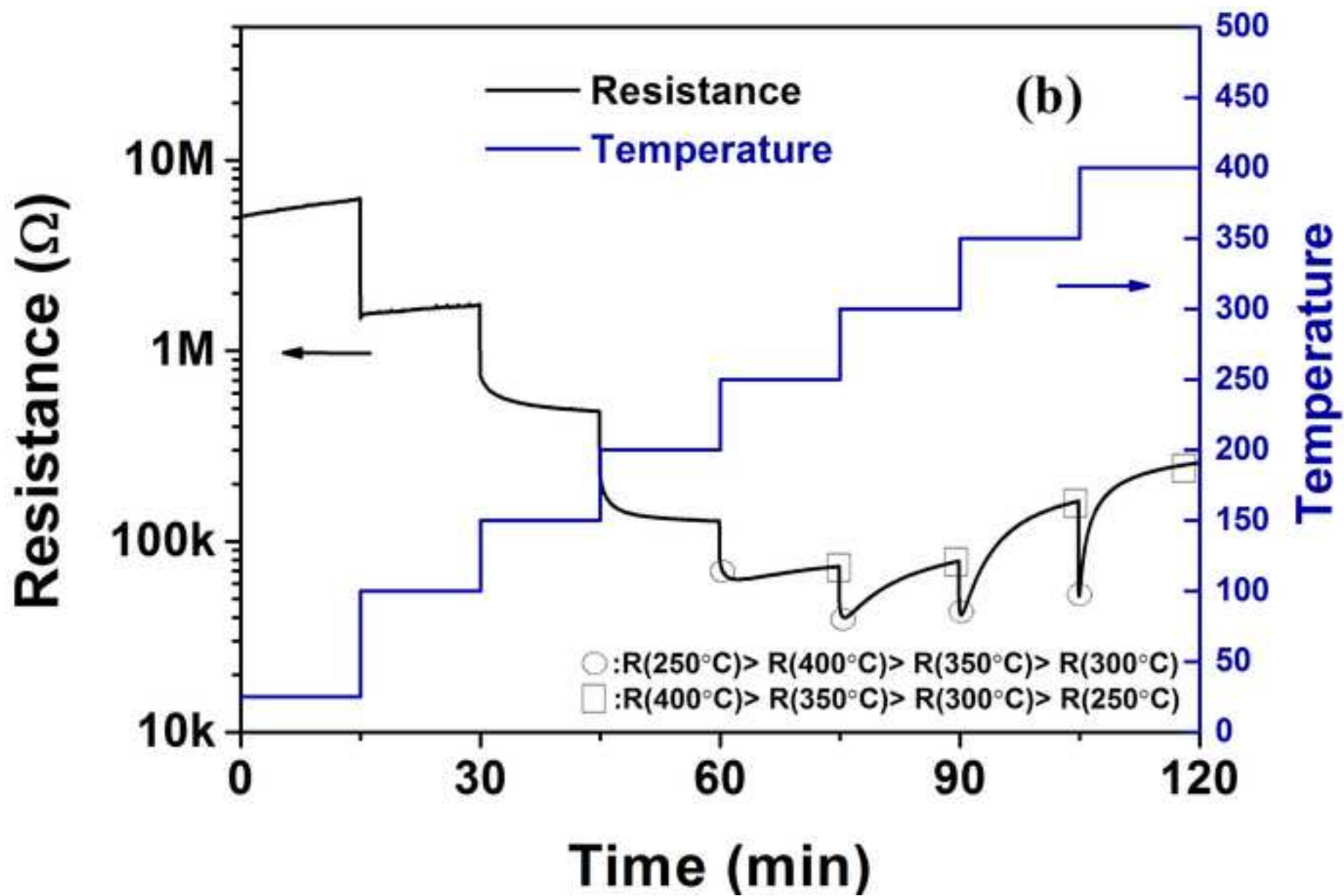


Figure(3a)  
[Click here to download high resolution image](#)



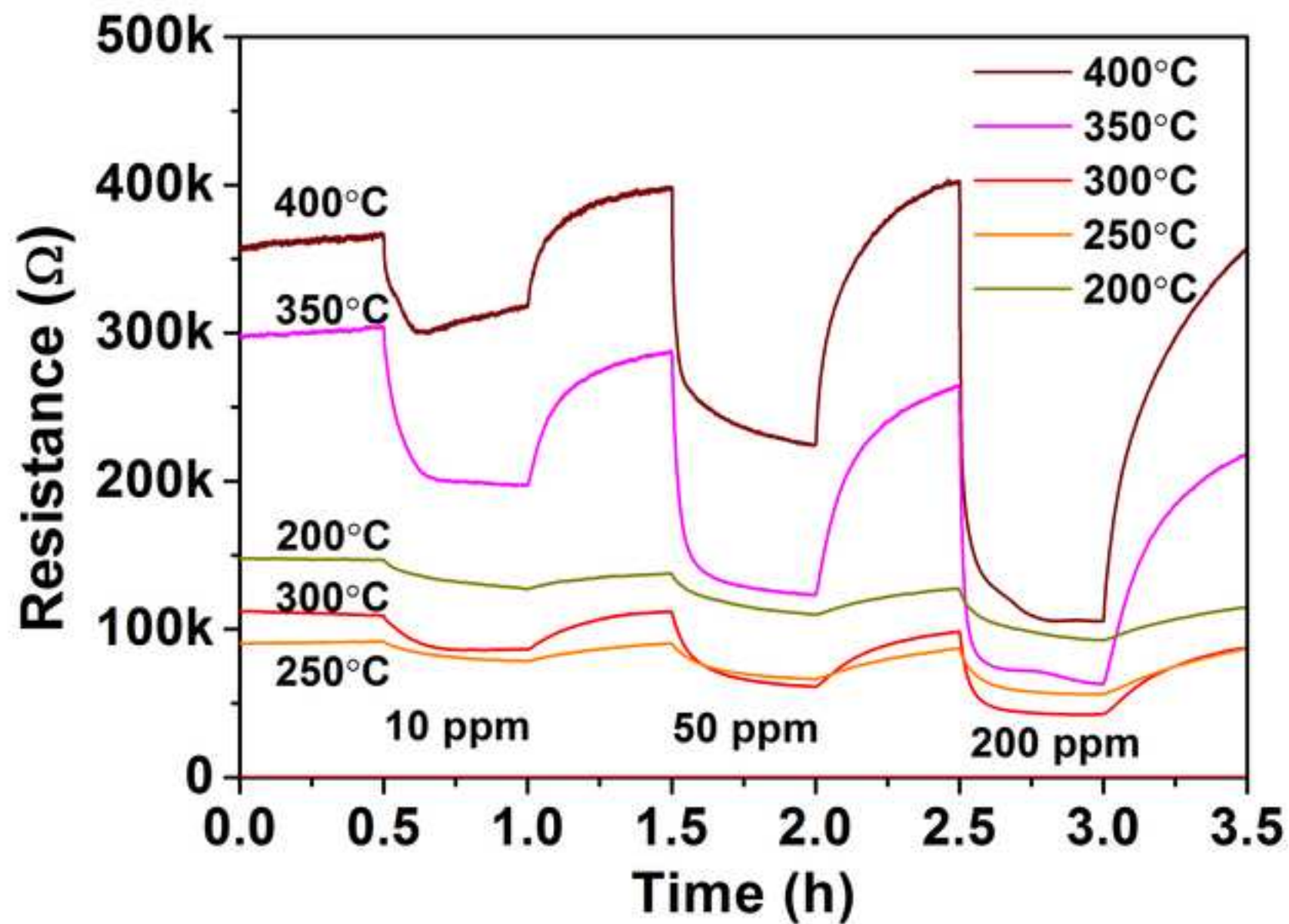


Figure(3b)  
[Click here to download high resolution image](#)



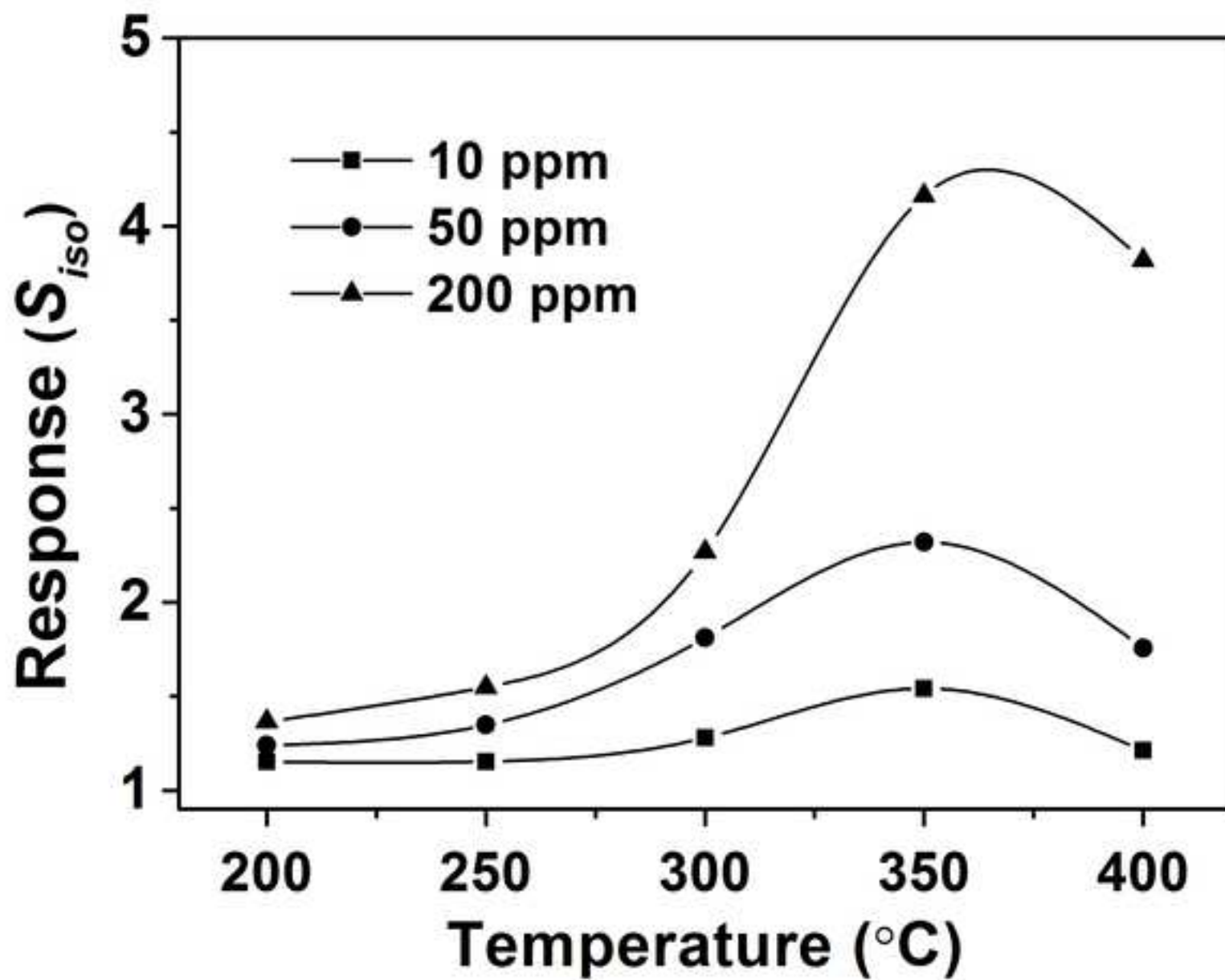
Figure(4)

[Click here to download high resolution image](#)



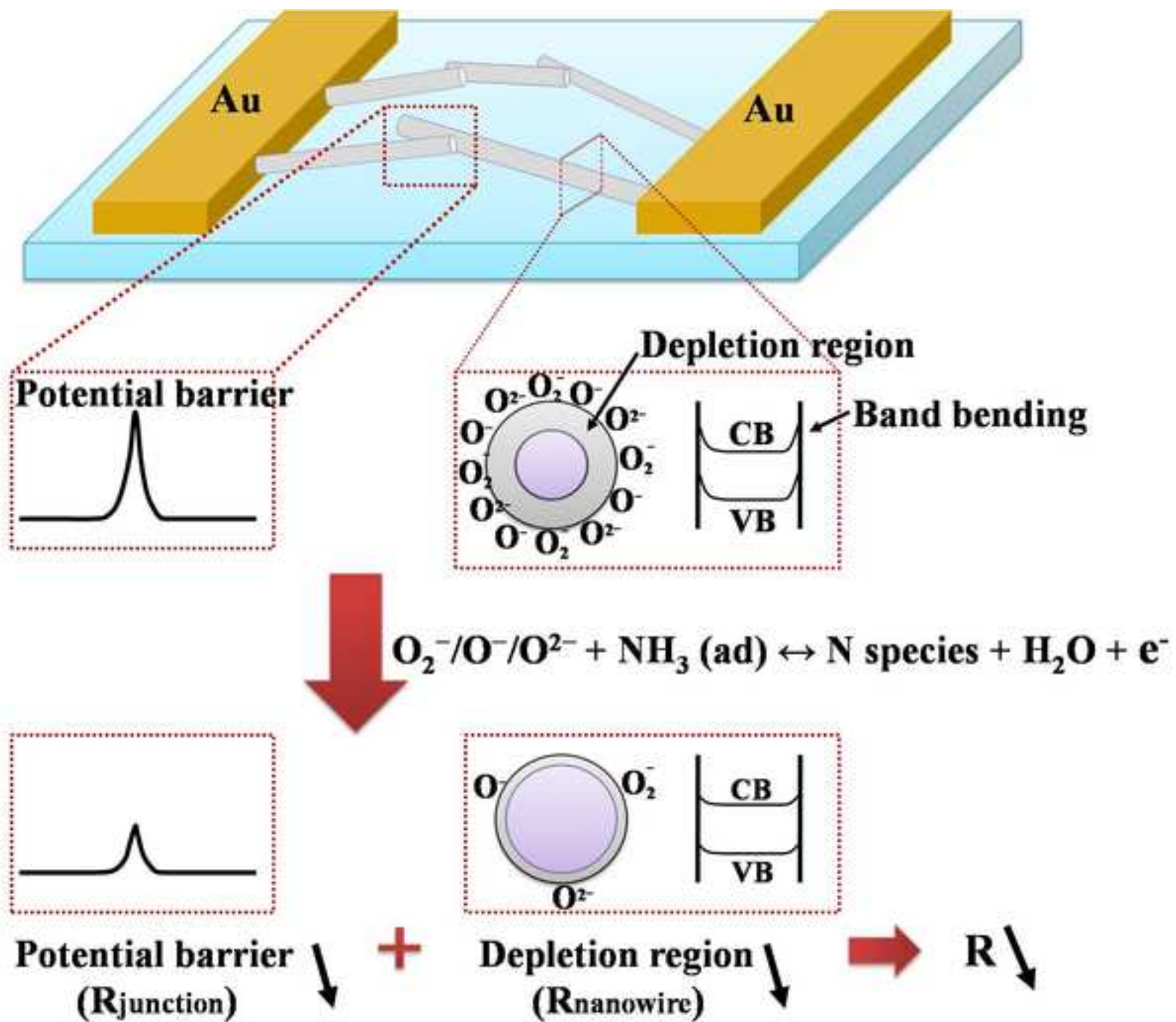
Figure(5)

[Click here to download high resolution image](#)

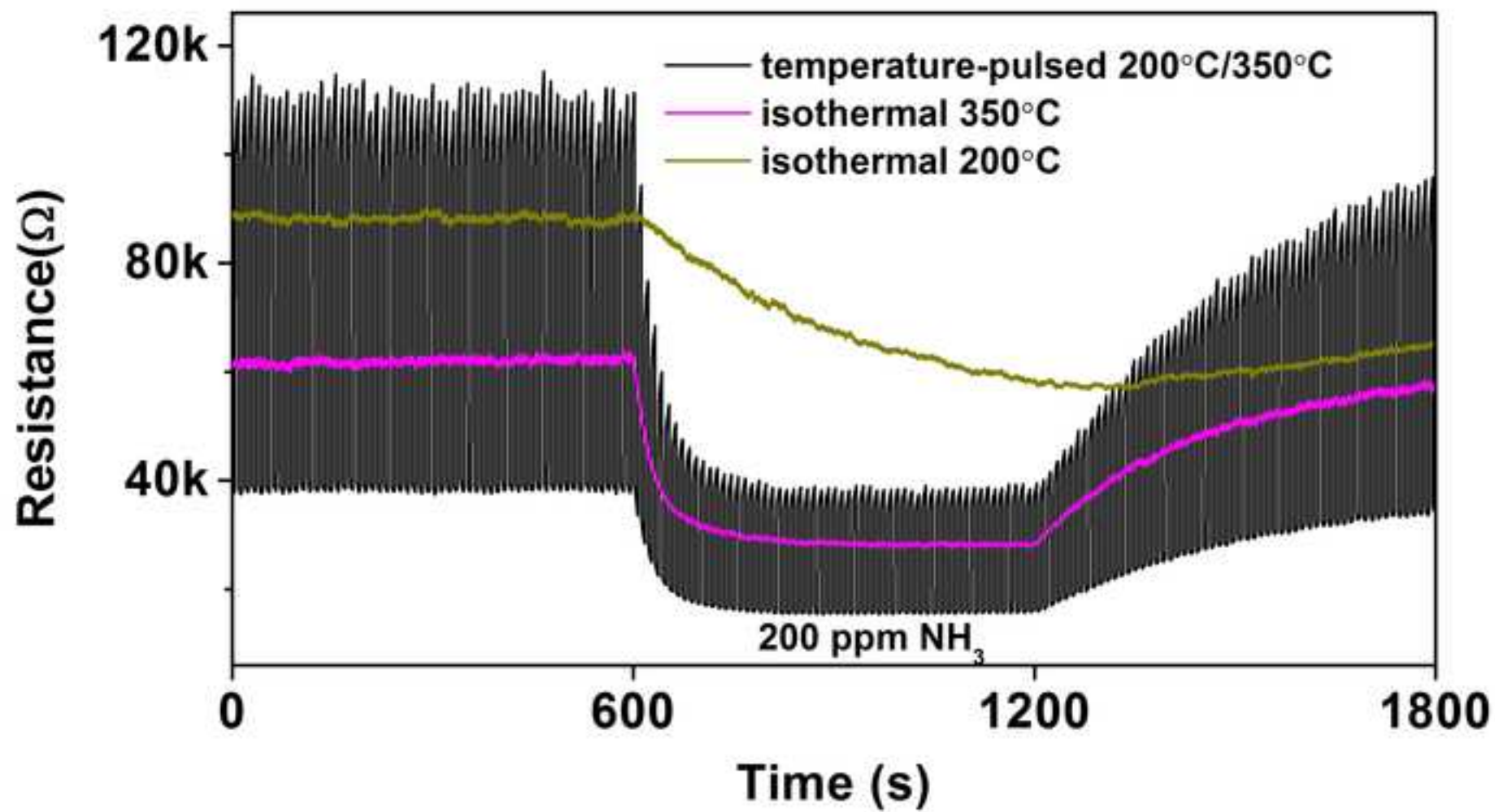


Figure(6)

[Click here to download high resolution image](#)

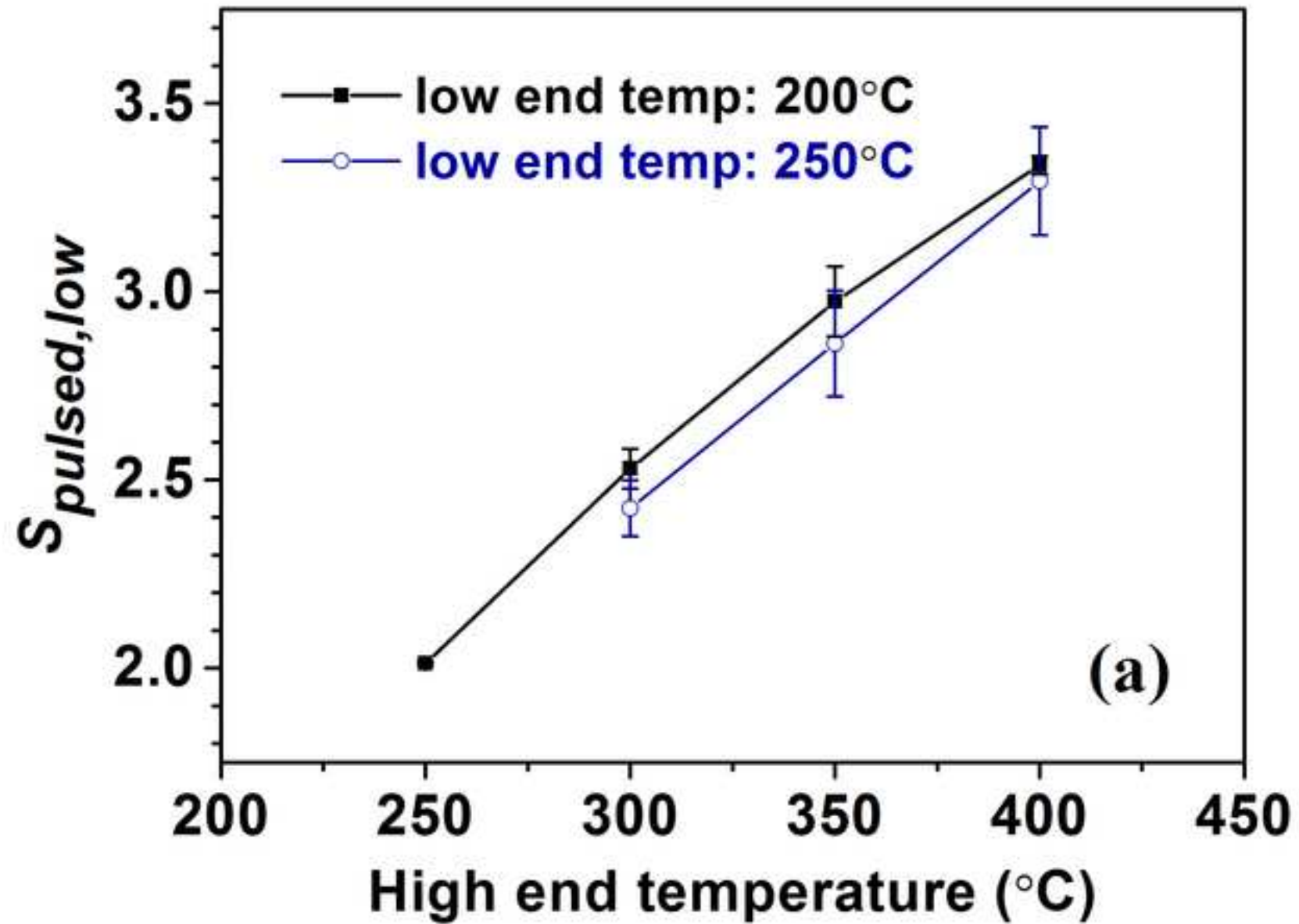


Figure(7)  
[Click here to download high resolution image](#)

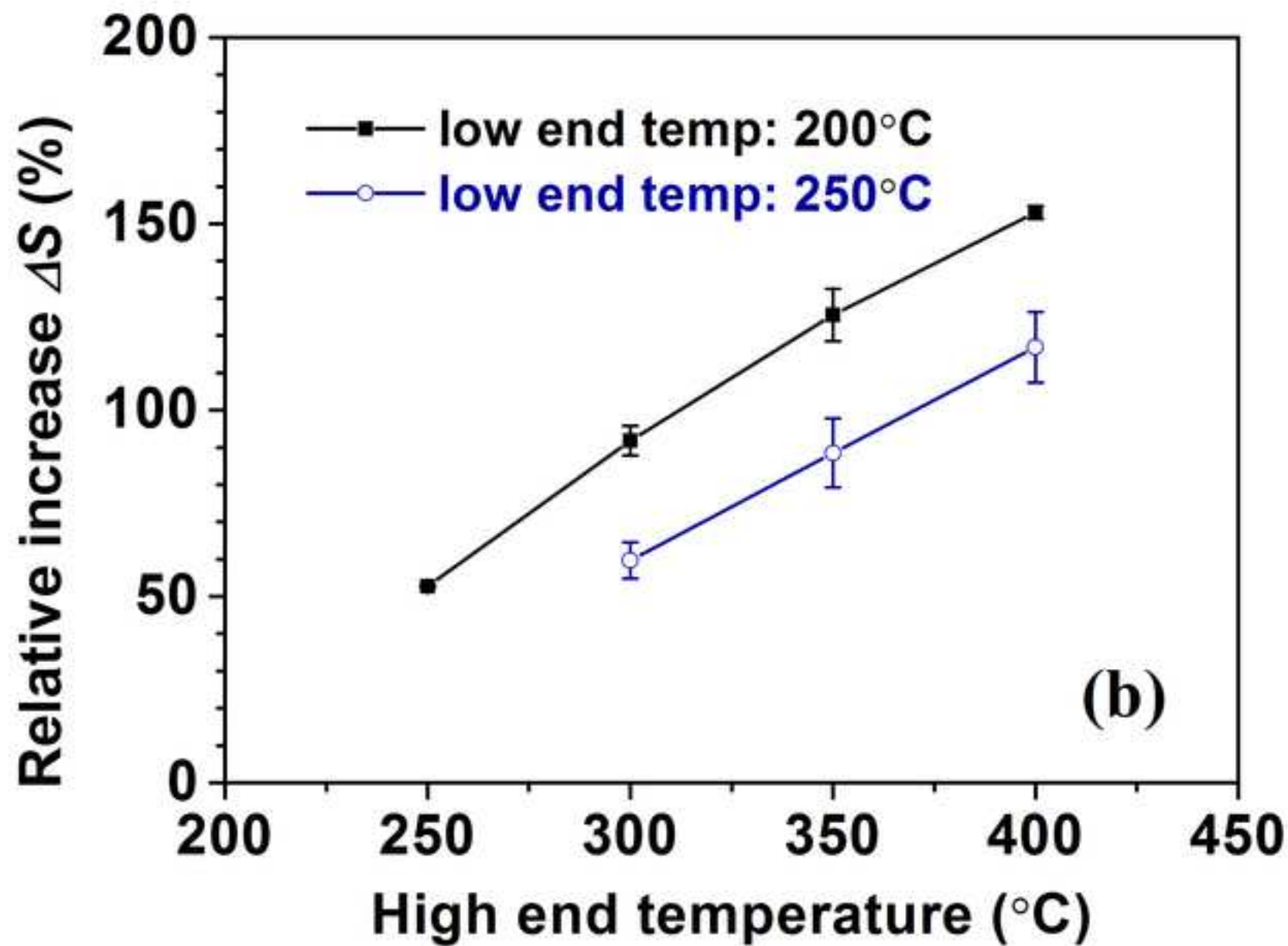


Figure(8a)

[Click here to download high resolution image](#)



Figure(8b)  
[Click here to download high resolution image](#)



**Supplementary Material**

[Click here to download Supplementary Material: Supplementary material revised II.docx](#)



## Vitae

**Feng Shao** graduated from Nanjing University of Aeronautics and Astronautics in 2006 and obtained an Msc degree from KTH Sweden in 2010. Then he conducted his research on nanowire gas sensors at Catalonia Institute for Energy Research and obtained his doctorate degree from the University of Barcelona in 2014. He is currently a postdoc at School of Electronic Science and Engineering, Nanjing University.

**Jian Dong Fan** conducted his doctoral research at Catalonia Institute for Energy Research and obtained his doctorate degree from the University of Barcelona in 2013. He has focused his research on metal oxide nanowires/nanotube based dye solar cells. He is currently a Postdoctoral researcher in Oxford University for perovskite solar cells.

**Francisco Hernández-Ramírez** graduated in Physics at the University of Barcelona in 2003 and obtained his Ph.D. at the same institution in 2007. He is actively involved in the development of innovative sensor prototypes based on nanowires. He has published more than 30 papers in peer-reviewed journals and contributed to five industrial patents.

**Cristian Fàbrega** obtained his PhD (2011) from University of Barcelona, devoted to the synthesis of titanium dioxide with nanostructured properties and their optical, electrical and electrochemical characterization for the generation of solar hydrogen using photoelectrochemical cells. He is a physicist and has a strong background on different characterization techniques such as Atomic Force Microscope, X-ray Photoelectron Spectroscopy, Electron Paramagnetic Resonance, Photoluminescence and Impedance Spectroscopy.

**Teresa Andreu** received her degree in chemistry at the University of Barcelona in 1999 and the PhD in 2004 in Material Science. From 2004 to 2006, she worked in the R&D Department of MacDermid Inc. involved in plating on plastics and electroless deposition of nickel. In 2007, she joined the Electronics Department of the University of Barcelona, mainly focused on the synthesis of metal oxides using nanotemplates. Since 2009, she is a researcher of the Advanced Materials Area of IREC. Her current interests include synthesis and characterization of semiconductors and its application to chemical sensors, photocatalysis and electrocatalysis.

**Andreu Cabot** was born in 1976 in Barcelona. He graduated in Physics in 1998 and received his PhD in 2003 (University of Barcelona). He did postdoctoral research at the University of California, Berkeley, under Prof. A. Paul Alivisatos' guidance. He returned to the Electronics Department, University of Barcelona in 2007 and joined the Catalonia Institute for Energy Research (IREC) in 2009 to form the Functional Nanomaterials Group. His research interests include the preparation, characterization and assembly of metal and semiconductor nanocrystals, to increase the efficiency and reduce the cost of current systems for energy conversion and storage.

**Joan D. Prades** was born in Barcelona in 1982. He graduated in Physics at the University of Barcelona in 2005 and obtained his Ph.D. at the same institution in 2009. He has experience in modelling of the electronic and vibrational properties of nanostructured metal oxides and in their experimental validation. He is actively involved in the development of innovative device prototypes based on nanowires. He has published more than 40 papers in peer-reviewed journals and contributed to more than 10 international conferences. He has also contributed to five industrial patents.

**Nuria López** (Barcelona, 1972) graduated in Chemistry with honours at the University of Barcelona, Spain (1995) and got her PhD degree in Theoretical Chemistry "cum laude" at the same university (1999), in the group of Prof. F. Illas. She then moved to the Center for Atomic-scale Materials Physics for her post-doc in the group of Prof. Jens K. Nørskov (Denmark). In 2001 she moved back to the University of Barcelona as a *Ramón y Cajal* fellow. In 2004 she was appointed Distinguished Professor by the DURSI in the junior category (under 41 years old). In November 2005 she took a position at ICIQ, where she currently leads a research group with focus on the theoretical research heterogeneous catalysis. She is also a part-time professor at the Department of Physical Chemistry of the URV. Núria has co-authored over 70 scientific publications. In September 2010 her "Tenure Track" period was successfully evaluated by an experts committee and she became a "Senior Group Leader" at ICIQ.

**Florin Udrea** is a professor in semiconductor engineering and head of the High Voltage Microelectronics and Sensors Laboratory at University of Cambridge. He received his B.Sc. from

University of Bucharest, Romania in 1991, an M.Sc. in smart sensors from the University of Warwick, UK, in 1992 and the Ph.D. degree in power devices from the University of Cambridge, Cambridge, UK, in 1995. Since October 1998, Prof. Florin Udrea has been an academic with the Department of Engineering, University of Cambridge, UK. Between August 1998 and July 2003 he was an advanced EPSRC Research Fellow and prior to this, a College Fellow in Girton College, University of Cambridge. He is currently leading a research group in power semiconductor devices and solid-state sensors that has won an international reputation during the last 20 years. Prof. Udrea has published over 350 papers in journals and international conferences. He holds 70 patents with 20 more patent applications in power semiconductor devices and sensors. Prof. Florin Udrea co-founded three companies, Cambridge Semiconductor (Camsemi) in power ICs, Cambridge CMOS Sensors (CCS) in the field of smart sensors and Cambridge Microelectronics in Power Devices. Prof. Florin Udrea is a board director in Cambridge Enterprise. For his 'outstanding personal contribution to British Engineering' he has been awarded the Silver Medal from the Royal Academy of Engineering.

**Andrea De Luca** graduated from the University of Naples Federico II (Naples, Italy) with a degree in Electronic Engineering in 2011, and is currently a Ph.D. student at the University of Cambridge (Cambridge, UK). His research interests include temperature sensors, thermal flow sensors, infrared emitters and detector for non-dispersive-infrared spectroscopy, micro-hotplate based gas sensors and nanomaterials for infrared absorption/emission enhancement and gas sensing. He is author or co-author of 15 publications in journals and conferences, and co-inventor of one patent application.

**Syed Zeeshan Ali** graduated from GIK Institute (Pakistan) in 2003 with a B.S. in electronic engineering. He completed his Ph.D. in 2007 at the University of Cambridge (UK) on the design of micro-hotplates for smart gas sensors and electro-thermo-mechanical modelling of membrane devices and was then a research associate at the University of Cambridge researching on micro-hotplates and gas sensing materials. He joined Cambridge CMOS Sensors (UK) in 2010 and is at present an R&D Leader at the company. His areas of research are microsensors and MEMS devices including gas sensors, IR emitters and IR detectors. He is the author or co-author of over 50 publications in international journals and conferences.

**Joan Ramon Morante** received his Ph.D. from the University of Barcelona in 1980. Since 1985 he is full professor in the Department of Electronics. In 2008 he joined the Catalonia Institute of Research for Energy, IREC where he is the head of the Advanced Materials Area. His activities have been centred in electronic materials and devices; the assessment of their related technologies and production processes, specially emphasizing materials technology transfer. He is actively involved in research of new sensors, actuators and microsystems.